Potentials and Limitations of CDMA Networks for Combined Inter-Satellite Communication and Relative Navigation

Rui Sun, Jian Guo, Eberhard Gill, Daan Maessen

Chair of Space Systems Engineering, Faculty of Aerospace Engineering
Delft University of Technology
Kluyverweg 1, 2629 HS, Delft, the Netherlands
r.sun@tudelft.nl, j.guo@tudelft.nl, E.K.A.Gill@tudelft.nl, D.C.Maessen@tudelft.nl

Abstract—**Precision formation flying missions require formation acquisition and maintenance through the interactions among spacecraft by the inter-satellite communication and relative navigation. This paper analyses the dedicated system constraints of the network architecture for precision formation flying missions. The critical time issue and the operational flexibility are found to be two main constraints. Potentially applicable architectures are discussed and evaluated, which combine different multiple access technologies, half-duplex/full-duplex configurations and network topologies. It is proven that the most suitable and efficient architecture for PFF mission is the use of the half-duplex CDMA with the topology that allows the role of being reference rotating from one spacecraft to another in different time slots. The capability of CDMA is also investigated in terms of the multiple access interference. The paper verifies that this interference can limit the maximum number of spacecraft and bounds the inter-satellite range diversity. The interference exhibits a Doppler dependency and suffers as well from the near-far problem. Inter-satellite navigation accuracy will easily drop down below meter level at the moments of zero- or n-kHz Doppler crossovers, and also in case of the signals being corrupted by the near-by interferences. Two realistic mission scenarios are provided to verify the severe effects of the interference. Operational considerations and interference mitigation methods are also recommended.**

Keywords-precision formation flying; communication; relative navigation; CDMA; Multiple access interference

I. INTRODUCTION

Precision formation flying (PFF) missions involve the acquisition and maintenance of spacecraft in a desired relative geometric configuration, especially when trying to create a large virtual spaceborne instrument, such as the applications in the field of remote sensing and radio astronomy. Coordinating the components of such instruments on separate spacecraft can require highly accurate relative orientation and positioning [1].

Commonly, PFF missions make use of a differential Global Navigation Satellite System (GNSS) approach by exchanging GNSS-based navigation measurements via the inter-satellite links. Yet this method is limited to Low Earth Orbit (LEO). Many missions such as PROBA-3, Darwin, Magnetospheric Multiscale (MMS) and Terrestrial Planet Finder (TPF) [2-5] require the spacecraft flying in a High Earth Orbit (HEO) or Lagrange points, where GNSS signals are very weak or are even not available. As a result, a

dedicated formation flying radio frequency (RF) technique using the locally generated inter-satellite ranging signals is necessary. The ranging capability is expected to integrate with the inter-satellite communication functionality for system efficiency. The use of the GNSS-like technology appears to be advantageous in such integrated system. Many missions that have been flown or proposed use this technology to assure a reliable inter-satellite communication and an accurate inter-satellite navigation, e.g., PROBA-3 [2], TPF [5], PRISMA [6] and MMS [7]. This paper also inherits the GNSS-like technology and regards it as a basic element to establish the PFF network.

In literature there are some discussions on the potential network architectures for formation flying. Bristow [8] proposed a concept called Operating Missions as a Note on the Internet (OMNI) that regards the spacecraft as network nodes and uses TCP/IP protocols to create a robust inter-satellite communications infrastructure. Similar proposals also include [9][10][11]. Vladimirova [12][13] discussed the potentials of applying WiFi or WiMax protocols for the establishment of the space wireless sensor network. An ability of implementing Ad-hoc has also been covered in order to support the high dynamics of spacecraft in large formations [14]. They all take advantages of the existing terrestrial protocols and try to move them to space. The benefits are the compatibility with the ground infrastructures and the good performance in terms of the large data throughput. However, the above two advantages are not the primary concern in PFF missions. The main requirement for the PFF inter-satellite link is to acquire and maintain the spacecraft in the desired relative geometry. The data exchanged should then be arrived timely to enable the estimations of the inter-satellite distance. This constraint is referred as to time critical issue in this paper and is elaborately analysed. Some of the existing terrestrial protocols will not be applicable due to the time critical issue. For example, WiFi, which functionally operates according to the detection of the medium [15], causes transmission uncertainty, which is a property that is unacceptable in PFF missions. This paper thus considers the medium access in fixed assignments of the possible connections by the classical multiple access (MA) technologies, such as Time, Code or Frequency Division Multiple Access (TDMA, CDMA or FDMA). Elaborate discussions on the choice of different MA technologies will be presented in this paper.

Another dedicated requirement for the PFF network is also proposed. It is the operational flexibility for

implementations across various mission phases. This requirement triggers the investigations on the choice of the network topologies and the half-duplex/full-duplex configurations. Considering all the above criteria, the paper will prove that the most robust and efficient manner in PFF missions is the use of the half-duplex CDMA with the topology that allows the role of being reference rotating from one spacecraft to another in different time slots.

The paper also discusses the limitations of implementing the CDMA concept. The well-known multiple access interference (MAI) will be introduced due to the non-perfect orthogonality of the Pseudo Random (PRN) codes. The Doppler dependency and the near-far problem are found to be two important factors that influence the MAI. The Dopplor dependency is severe when the Doppler offset between two spacecraft is close to zero or multiple integers of kHz. This is referred to as zero-Doppler crossover [16] and n-kHz Doppler crossover [17]. Server effects of the Doppler crossovers are investigated, especially in the situation where there is also a near-far problem. The resultant MAI error is analytically derived and verified using software simulations. Two case-study scenarios are used to determine the level of the MAI error and to predict the occurrence of the significant errors within an entire orbit period in realistic formations.

The paper shows several contributions, on the investigation of the possible network architectures, on the theoretical analysis of the selected CDMA strategy, on the analytical characterization of the MAI errors, and on the practical evaluation over two realistic missions.

The paper is organized as follows. In Section II, the inter-satellite communication and relative navigation system is introduced in order to propose the dedicated constraints for PFF network in Section III. Candidate network architectures considering different MA technologies, half-duplex/full duplex configurations, and network topologies are discussed and evaluated in Section IV. Then, network capability in terms of MAI is analysed, followed by an error characterization with respect to the Doppler offset and the near-far problem in Section V. In Section VI, two case-study scenarios are provided to identify the error level of MAI and to predict the occurrence of significant errors in realistic formations. Section VII concludes the paper and provides recommendations.

II. INTER-SATELLITE COMMUNICATION AND RELATIVE NAVIGATION SYSTEM

The inter-satellite system for PFF missions shall integrate communication and relative navigation into one package. Inter-satellite navigation is based on the locally generated inter-satellite ranging signals. A cost effective manner to generate these signals is to modify an existing GNSS receiver such that it can operate as a transceiver. The ranging method traces heritage to the GNSS-like technology and results in a highly miniaturized and accurate ranging device.

Such an inter-satellite system is expected to satisfy some specific high-level requirements according to the proposed missions [5][6]. According to these requirements and assuming the system operating in S-band 2.2 GHz, the EIRP

(Effective Isotropic Radiated Power) is around 3 dB and the space loss is -129 dB. With the noise at the level of -134 dB of using 5 MHz bandwidth, it can be easily demonstrated that the received signals is 7 dB above the noise.

- Communication and relative navigation are integrated into one package, with mass less than 2 kg, and power consumption less than 2 W;
- Operating range less than 30 km;
- Omni-directional (4π steradian) coverage;
- Flexible to implement across various phases of mission operations in two modes: deployment, reconfiguration and collision avoidance tasks are achieved through the coarse-mode; formation maintenance in the desired configuration is required in fine-mode for scientific proposes;
- Navigation accuracy is in meter level for coarse-mode using code measurement (pseudorange) only, and centimetre level for fine-mode using the combination of code and carrier phases;
- Measurement update rate ≥ 1 Hz.

Space System Engineering group (SSE) in Delft University of Technology (TUDelft) has developed a software-defined inter-satellite communication and navigation simulator, which currently implements the signal generation and processing on PC via Matlab based on the system functional block in Figure 1. As shown, it comprises the transmitter and receiver front-end, signal generator and signal processing. The front-end comprises signal amplifier, band pass filter, down-conversion, sampling, and quantization. Frequency synthesizer is used in order to synchronize the edges of clocks in PRN code chipping frequency, and carrier and intermediate frequencies. The signal generator is used to generate carrier and GPS-like PRN code modulated signals. In single processing, acquisition, tracking and decoding modules are included for data recovery, code and carrier phase extraction, and pseudorange (-rate) derivation.
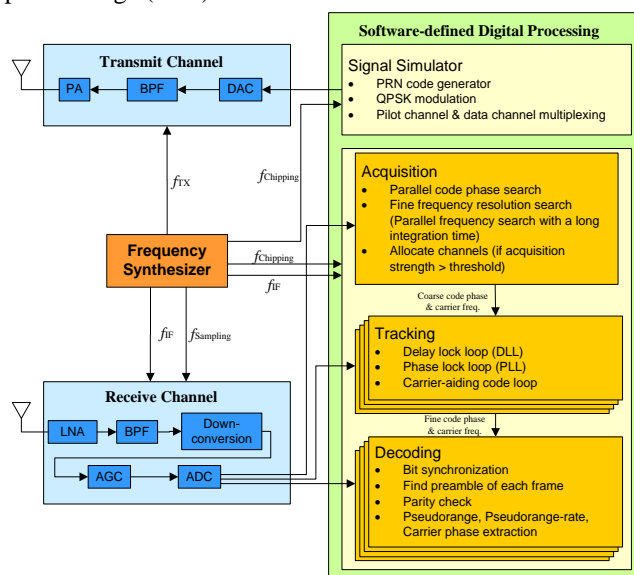

Figure 1.   Inter-satellite communication and navigation system functional block diagram

Figure 2 depicts the signal generation and processing simulations assuming an intermediate frequency (IF) of 9.548 MHz and a sampling rate of 38.192 MHz. In the signal generator, the GPS C/A code is used as pseudorandom code,with a chipping rate of 1.023 Mcps and length of 1023 chips. The Doppler shift is assumed following a linear function relative to the simulation time.

The auto-correlation property, as shown in Figure 2(a), allows for accurate range measurements by yielding a sharp peak only when the replica code delay in the receiver is perfectly aligned to the code delay of the incoming signal. The signal energy is wideband spread due to the noise-like characteristic of the PRN code. PRN code spectrum is shown in Figure 2(b). The acquisition process, in Figure 2(c), is a global search in a two dimensional search space for approximate values of Doppler shift and code phase. This process is time and computation consuming. Therefore, parallel code/frequency one-dimensional search using Fast Fourier Transform (FFT) is implemented. After acquisition, control is handed over to the delay lock loop (DLL) and the phase lock loop (PLL). The fine estimates of the code and carrier phases will be obtained continuously after DLL and PLL. The variations due to the dynamics between spacecraft will also be tracked. As can be seen in Figure 2 (d) (c), in DLL, code error is ultimately reaching zero when the loop is getting to steady state, while in PLL, the linear function of Doppler is well represented. Communication bits in Figure 2 (e) are extracted from the tracking loops.

### III. CONSTRAINS ON PFF NETWORK ARCHITECTURE

The time-critical issue and the operational flexibility are found to be two important criteria in PFF missions.

A. Time-critical requirement

Time-critical requirements are driven by the nature of tight control, collision avoidance or scientific needs in some specific operational periods in PFF mission. These periods shall require high navigation accuracy and high measurement update frequency.

A relative navigation filter (e.g., extended Kalman filter) is used to account for the relative position errors resulting from all relevant non-modeled accelerations acting on the spacecraft. This process employs a numerical integration scheme in the filter that is updated at discrete intervals (t_i) as illustrated in Figure 3. The estimated relative state vector is obtained from an interpolation of the previous cycle. Based on all the measurements between t_i and t_{i+1}, a continuous polynomial representation of the trajectory is made available, which serves as starting point for the next filter update and relative orbit prediction [18]. Obviously the propagation period t_i-t_{i-1} has to be small for better approximations of the relative state vectors. On the other hand, t_i-t_{i-1} is limited by the processing time Δt_{proc}. Its typical value is 30 s for low earth orbits. In deep space, this period can be extended to several minutes or longer.

The measurements used in the filter are provided by the inter-satellite system. They can be either the unambiguous coarse code or the ambiguous precise carrier phases. Figure 4 exhibits their update timelines.

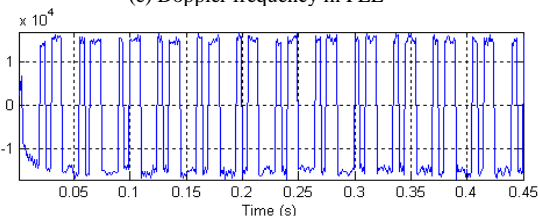(a) Auto-correlation of PRN code

(b) PRN code spectrum
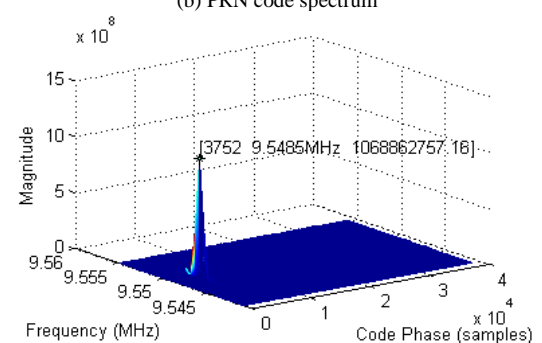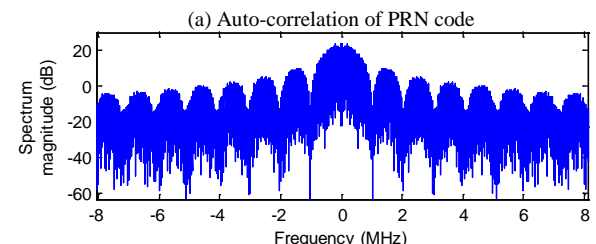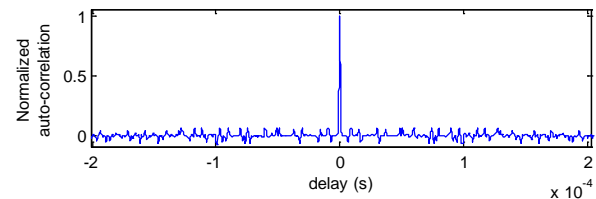
(c) Acquisition results. The peak is present at the point where the code delay is at 3752 sample (38192 samples in total for one complete PRN sequence) and carrier frequency is at 9.5485 MHz. That is, Doppler shift is approximately 500 Hz.
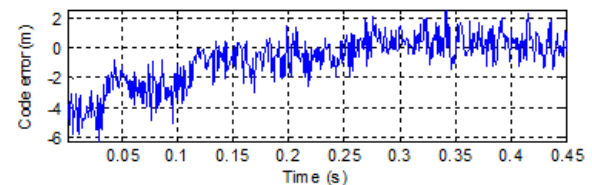
(d) Code error estimation in DLL
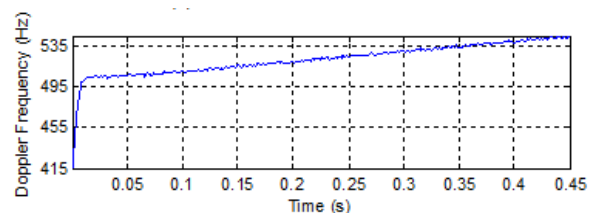
(e) Doppler frequency in PLL

(f) Communication bits extraction. The values are not ±1 because of the quantization in the front-end and integration in the tracking loops.

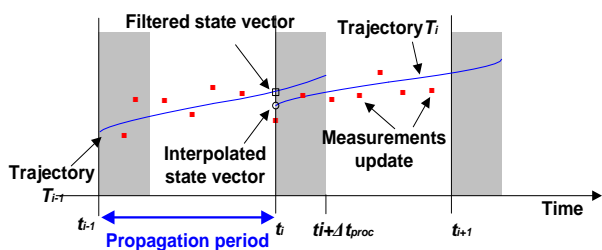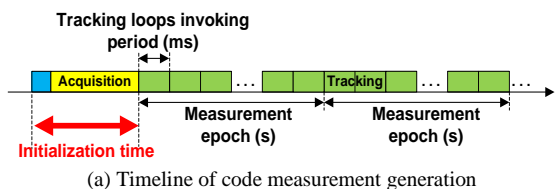Figure 2. Software-defined signal generation and processing results

Figure 3.   Timeline of relative navigation filter

(a) Timeline of code measurement generation

(b) Timeline of carrier phase measurement generation

Figure 4.   Timeline of code and carrier phase measurements generation

It is observable in Figure 4 that the measurements are yielded after different initialization time, including the acquisition process for both of the codes and carrier phases, and some extra time only for the carrier phases to calculate the integer ambiguities and multipath corrections.

In the acquisition process, a long integration is performed to achieve sufficiently high carrier to noise ratio.

For integer ambiguities resolution, an sufficient large change of the relative geometry between spacecraft is normally required [6], which consumes long time. It is even more time consuming if the carrier phase itself is contaminated by multipath. For example, the integer ambiguity resolution used by PRISMA mission is to rotate a spacecraft for solving the line-of-sight (LOS) ambiguities firstly and then the distance ambiguities subsequently, taking 5 mins and 10 mins, respectively [6]. The resolution is combined with tabulated multipath correction through a filtering and smoothing process [6].

After initialization, tracking will be continuously running until the link is broken when switching the communication channel from one pair of spacecraft to another pair in a formation. At that time, re-initialization needs to be performed, including the corresponding initialization of sensor acquisition and carrier phase integer ambiguity resolution. This process consumes precious time and could result in a period that the on-board relative navigation filter in Figure 3 is propagating the dynamics for a couples of minutes without the measurement updates. The impact of

such switching thus leads to an unsatisfactory performance of the navigation filter, which is unacceptable especially when the tight control is required at that specific time for the relative geometry maintenance.

This issue is referred to as time-critical constraint. The following PFF network architecture design should accommodate such time-critical constraint and give a high priority to timeliness instead of traditional considerations on the data throughput.

B.   Flexible operations across all mission phases

Another important consideration of PFF networking is to recognize that the relative navigation requirements will change during the course of the mission's operations. The inter-satellite system is expected to operate across various phases of formation precision, requiring different levels of position sensing and control maneuvering.

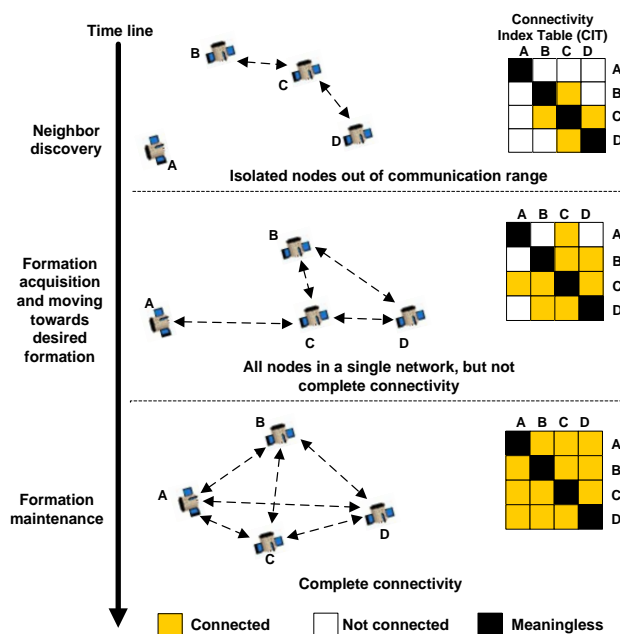Figure 5 illustrates the revolutionary phases of a PFF mission.

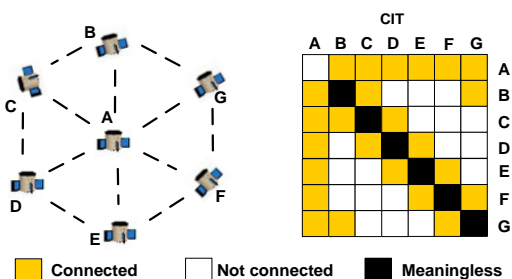Figure 5.   Evolutionary phases of a PFF mission

Figure 6.   An example of complete connectivity with seven spacecraft in formation

In the initial deployment where the spacecraft are separated by substantial distances from one another, the resolution of position and orientation data are based e.g., on

coarse-mode sensors for collision avoidance, enabling further movement toward the desired configuration to take place safely. Spacecraft can be seen as free flyers located at a wide range of inter-satellite distances to each other. They will randomly access to the network. Neither a solely centralized nor a distributed topology is efficient in such situation, as some spacecraft are possibly out of the communication range of others.

As the spacecraft continue to aggregate into the desired spatial arrangement, they will eventually discover other spacecraft, which may be itself isolated or be already a member of a multi-spacecraft network. This condition, defined as formation acquisition and depicted in the centre of Figure 5, is in progress until all spacecraft are connected in a single network and moving towards desired formation.

Finally, when all spacecraft in the system show a "complete connectivity" and are settled into the desired pattern, formation maintenance are performed as shown in the bottom of Figure 5. Typically, a higher accuracy of their relative position is acquired, enabled by switching the inter-satellite system into the fine-mode. A precise formation may then be achieved using tighter control loops. Science operations will take place for e.g., multiple point remote sensing. At this moment, the mission topology will evolve to a centralized graph with one spacecraft at least chosen being the reference for a certain time period for relative navigation and formation control.

It is noted that in this final topology, "complete connectivity" does not mean all spacecraft must connect to each other, but connect to the desired spacecraft (normally the closed ones), which satisfies certain formation configuration. This happens especially in a large scale network such as depicted in Figure 6.

Subsequently, PFF can be reconfigured to set up a new arrangement for another science objective. The reconfiguration operation may drop back to coarse formation mode and prepares for new configuration, whereupon precise formation can again be executed [19].

A connectivity index table (CIT) is proposed to be part of traffic exchanged among spacecraft to share the current network condition. The measured range can also be included in the CIT, in which way a spacecraft will know all the relative positions even though not all of them are directly connected.

IV. NETWORK ARCHITECTURE FOR PFF

As a result of time-critical issue, networking solutions prefer the network nodes in a fixed assignment for all possible connections by MA technologies TDMA, CDMA, FDMA or their combinations, since they enable each spacecraft providing measurements from each of the others equally and timely [20].

In addition, the choices of half-duplex/full-duplex configurations and centralized/distributed topologies also play important roles in PFF network architecture.

Inevitably, if transmitting and receiving happen at the same time, some of the transmitted signal will leak into the receiver front ends and may easily saturate the receiver front ends or otherwise overwhelm the external signals. Half-

duplex transceiver enables the transmitter and receiver taking turns to work, in which way "self-signals" are avoided. Full-duplex transceiver uses an appropriate filter to isolate the transmitter and receiver at their separated frequency bands to reject "self-signals". If the navigation measurements are not required simultaneously and continuously, half-duplex configuration is adequate and power-saving.

Network topology is expected to operate in a flexible arrangement, so as to account for the evolutionary phases of a PFF mission as shown in Figure 5. Neither solely centralized nor distributed topology is efficiently applicable during the neighbor discovery and formation acquisition phases, because some spacecraft are possibly out of communication range of others and could not access to the network. As the spacecraft progress towards the desired formation, it is better for the topology to evolve to a centralized graph in order to enable at least one spacecraft as reference for precise relative navigation and formation control. The role of reference can rotate from one spacecraft to another to avoid the problem of single point of failure.

Roles rotating at different time slots will give a robust and efficient connectivity. It can be implemented in a TDMA sequence with a strict timing boundary or a CDMA configuration with an adjustable period of time slot. Constraints of operating any of them come from the time-critical navigation requirements.

The possible combinations of different MA technologies, half-duplex/full-duplex configurations, and network topologies for PFF missions are illustrated in Figure 7-9.
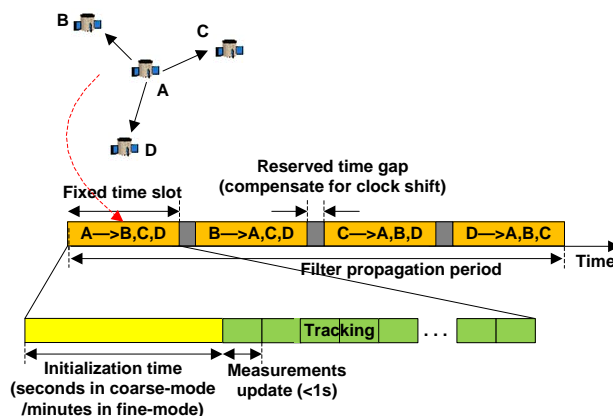

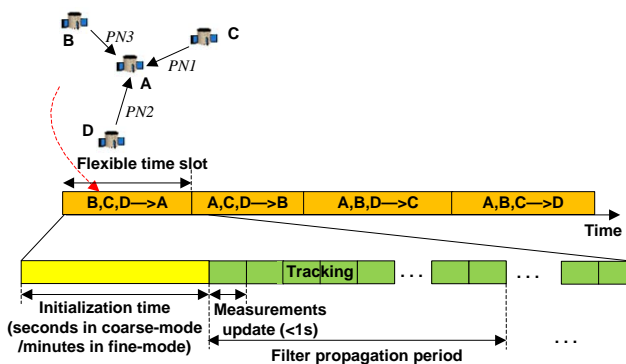Figure 7.   Half-duplex TDMA implemented for PFF mission

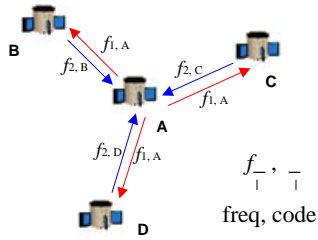Figure 8.   Half-duplex CDMA with roles rotation in PFF missions

Figure 9.   Full-duplex CDMA implented for PFF missions

In half-duplex TDMA mode in Figure 7, the measurements for propagating relative dynamics are from all of the spacecraft at different strictly fixed time slots. Therefore, the time slot is limited by the filter propagation period. That is, if a complete duty cycle of one TDMA sequence is as long as propagation period t_i-t_{i-1}, the time slot will be one-quarter of t_i-t_{i-1} (in four spacecraft formation), or even smaller to compensate for the clock drift by reserving a time gap between two slots. There is thus a high possibility that the time slot arranged to each spacecraft is too short to implement carrier phase measurement and the associated integer ambiguity resolution. This circumstance in TDMA mode can be improved by extending the propagation period, or equivalently, allowing the filter to freely propagate without measurement updates. However, the price of an increased relative navigation error has to be paid.

The fixed time slot of TDMA also limits the ability of working during different mission phases. It is caused by the variable inter-satellite range diversities and variable ranging accuracy requirements along with the course of the mission's operations.

Therefore, it is better to have an adjustable time slot and propagation period to avoid signal collisions and also guarantee efficient channel occupations and successful ranging abilities. Half-duplex CDMA with roles rotating architecture is thus proposed in Figure 8. It provides better capabilities in a way that the complete measurements from all of the spacecraft can be obtained in a single time slot by the use of CDMA strategy. This renders the duration of this time slot more flexible. It can be long enough to resolve the ambiguities and allow re-acquisitions. The implementations of either coarse-mode or fine-mode ranging at different mission phases are also possible as the time slot is adjustable. In addition, the signals transmitted from other spacecraft are not necessary to start at the same time in this CDMA mode, thus, it is tolerable if a spacecraft is joining in or dropping out of the formation.

Another advantage of such CDMA technology is that it can use the GNSS-like technology to the largest extent. For example, multiple channels in the system can work simultaneously. Differential measurements can be considered to improve ranging accuracy.

As comparison, another candidate architecture using full-duplex CDMA in centralized topology is shown in Figure 9. The isolation between transmitter and receiver is realized by separated frequencies and appropriate filters. It takes the advantages of allowing the signal transmissions among spacecraft without the necessity of re-acquisition each time at different time slots. Therefore, the measurements in this architecture can be processed simultaneously and continuously. The time-critical requirement is satisfied in an extreme solution that is the continuous connectivity. In addition, this method benefits from the fact that both clock offset and relative distance can be produced using dual one-way ranging [21].

However, the flexibility is low for this full-duplex CDMA strategy as it uses a centralized topology within the entire mission lifetime. The nature of full-duplex configuration needs more complicated system and consumes more power.

Considering all the above advantages and drawbacks for the three different architectures in Figure 7-9, half-duplex CDMA with roles rotating is the most robust and efficient manner for the PFF missions. The benefits of using it has been explained above. The following sections will focus on its limitations, including the well-known near-far problem and multiple access interference.

V.   CDMA PFF NETWORK CAPABILITY: MULTIPLE ACCESS PERFORMANCE AND NEAR-FAR PROBLEM

The multiple access capability of CDMA is achieved by using the GNSS-like C/A code. However, it is not a completely orthogonal signalling format, which means cross-correlation is nonetheless present and induces noise in terms of MAI.

A.   Cross correlation without Doppler effects

Assume that there are two signals, which are all un-correlated PRN codes with identical spectrum $G_s(f)$ and received at the same power level of P_s. The MAI term is introduced due to cross-correlation (CC) between undesired signal $c_m(t)$ and desired reference signal $c_k(t)$, where $c(t)$ represents PRN code. Ignoring the data modulation, Doppler frequency differences and noise for the moment, the MAI term is $c_k(t-\tau_k)c_m(t-\tau_m)$ with code delay τ_k, τ_m. Its power spectrum $G_{MAI}(f)$ is thus obtained by convolving the individual signal spectrum $G_s(f)$ [22]:

$$G_{MAI}(f) = P_s \int G_s(f)G_s(v-f)dv \qquad (1)$$

Only the MAI spectrum near $f=0$ is important because the correlation filters have a small bandwidth on the order of Hz. $G_s(f)$ is in the form of $sinc^2$, thus [22]:

$$G_{MAI}(0) = P_s \int G_s^2(v)v = P_s \int_0^\infty \left(\frac{\sin \pi f / f_c}{\pi f / f_c} \right)^4 df = \alpha \frac{P_s}{f_c} \quad (2)$$

where f_c is chipping rate, α is a coefficient as a function of the filtered spectrum of $sinc^2$. If the spectrum includes all of its sidelobes, α is 2/3. If the spectrum is filtered to include only the mainlobe, α increases to approximately 0.815 [22].

Assuming *M* spacecraft at the same separation distances with the reference satellite in the formation, then *M-1* interfering multiple access signals exist. Considering white noise with noise spectrum density of N_0, the equivalent noise density and the effective energy per bit to equivalent noise density ratio are:

$$N_{0eq} = N_0 + \alpha(M-1)P_s / f_c \qquad (3)$$

$$\frac{E_b}{N_{0eq}} = \frac{PT_d}{N_0 + \alpha(M-1)P_s / f_c} \qquad (4)$$

where $T_d = 1/f_d$, f_d is data bit rate. E_b/N_{0eq} determines the bit error rate. It is on the order of 10 dB if BER=10^{-5} and BPSK modulation without error correction coding is employed.

Furthermore, taking into account of the various separation distances between spacecraft, the near-far problem shows up. The effective E_b/N_{0eq} from a remote transmitter is further reduced due to the increase of MAI in close proximity. Because the free space loss is proportional to the square of distance, MAI spectrum density in eq. (2) is consequently multiplied by R_f^2/R_n^2, a factor to indicate the far desired signal to the near undesired interference range-squared ratio. E_b/N_{0eq} can then be revised to:

$$\frac{E_b}{N_{0eq}} = \frac{PT_d}{N_0 + \alpha(M-1)(R_f^2 / R_n^2)P_s / f_c}$$

$$= \frac{P_s}{N_0 f_d (1 + \alpha(M-1)(R_f^2 / R_n^2)P_s / (f_c N_0))} \qquad (5)$$

$$= \frac{E_b}{N_0} \frac{1}{(1 + \alpha(M-1)(R_f^2 / R_n^2)P_s / (f_c N_0))}$$

The multiple access effect of *M-1* near interferences degrades the original E_b/N_0 by a factor of $1 + \alpha(M-1)(R_f^2/R_n^2)P_s/(f_c N_0)$. Note that signal to noise ratio P_s/N_0 equals to $f_d \cdot E_b/N_0$. Figure 10 displays the difference between the original E_b/N_0 and E_b/N_{0eq} caused by MAI effects. Assume using C/A code with chipping rate f_c of 1.023 Mcps, data bit rate f_d is 2 kbps, original E_b/N_0 is 10 dB, and coefficient α is 0.815 in case of 2 MHz bandwidth front-end filter by taking account of only the mainlobe spectrum.

As shown, in case of a small scale network and small distance diversity, e. g., only one or two interfering satellites in the near field of view, the difference between E_b/N_0 and E_b/N_{0eq} is less than 1 dB and can be negligible. However, as the number of satellites is getting larger or the far desired signal to the near interference range ratio is getting higher, this difference could be beyond the original E_b/N_0 threshold, which is unacceptable.

The impact factors of MAI, in the sense of the degradation of E_b/N_0, can be translated to:

- Maximum operating range diversity at a specific number of satellites in formation;
- Maximum achievable number of satellites in a formation that has low inter-satellite distance diversity.

For example, if five satellites in formation, one behaves like a reference and receives signals simultaneously from the other four. The maximum operating range is then in the sense that inter-satellite distance ratio could not be larger than 14 (red line in Figure10). On the other hand, if assuming the distance has only 3 times diversity, the maximum achievable number of satellites can be up to 620.
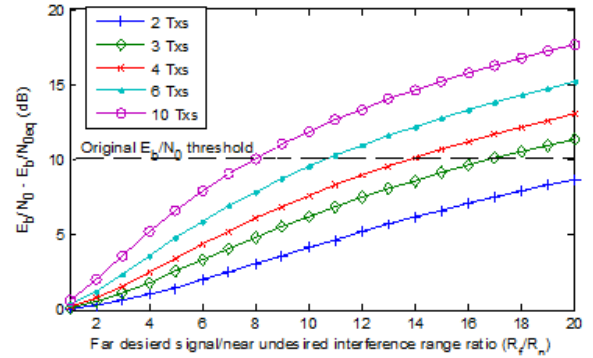

Figure 10. Difference between the original E_b/N_0 and E_b/N_{0eq} due to the near-far problem

Nevertheless, the results here are much more focused on communication performance and based on the assumption that Doppler effects on cross-correlations are ignored. When it comes to inter-satellite navigation, Doppler effect should be counted in, as significant errors will show up even in a small scale of network with low separation diversity.

B. Cross-correlation at high Doppler Offset

When taking into account of the different Doppler frequencies on the signals, there are Doppler frequency offsets on the cross correlations. The difference between two Doppler frequencies Δf_k, Δf_m for the desired and interference signals will be referred to as the Doppler offset $\Delta f_{m,k}$.

Without considering Doppler, the strongest and average cross-correlation peaks are approximately -24 dB and -30 dB lower than the main auto-correlation peak [23]. However, higher Doppler offset could exacerbate cross-correlation levels to -21.1 dB [23].

Specifically, for higher Doppler offset $\Delta f_{m,k}$, the cross-correlation term turns to

$$R_{cc} = \int_{(k-1)T}^{kT} c_k(t-\tau_k)c_m(t-\tau_m)\cos(2\pi\Delta f_{m,k}t + \Delta\phi_{m,k})dt \qquad (6)$$

where *T* is integration time. The interference code structure $c_m(t)$ is changed by multiplication with $\cos(2\pi\Delta f_{m,k}t + \Delta\phi_{m,k})$. The effect of this multiplication can be significant when the Doppler offset is close to zero, then cross correlation errors become significant. This phenomenon has been observed and demonstrated by

researchers and was referred to as Doppler crossover [23][24].

Furthermore, PRN code (e.g., C/A) is not continuous but 1023 chip length sequence periodically repeated every 1 millisecond. That results in 1 kHz ($f_c/P = 1.023Mcps/1023$) separated lines in the spectrum within $sinc^2$ envelope [22]. Thus, for non-zero Doppler offset $\Delta f_{m,k}$, the spectrum of $c_m(t)$ is shifted with frequency $\Delta f_{m,k}$. If $\Delta f_{m,k}$ is not close to the integer multiple of 1 kHz, the line components of the desired signal spectrum and the shifted interference signal spectrum does not overlap, thus the cross correlation spectrum by convolving them $G_{m,k}(f) = \int G_k(f)G_m(v - (f + \Delta f_{m,k}))dv$ will diminish. On the contrary, mixing at the existing line frequencies on the order of several kHz will result in the interference being minimally suppressed. That is, if Doppler offset is an integer multiple of line component spacing 1 kHz, cross-correlation noise energy "leaks" through the correlation process, and could exacerbate cross-correlation levels to -21.1 dB [23]. The cross correlation errors in this case behave similarly to the zero Doppler crossover scenario, and have been regarded as n-kHz Doppler crossover [16].

In order to estimate the magnitude of the cross-correlation errors, the ranging system work process needs to be understood. As shown in Figure 1, in the tracking loops of DLL and PLL, three correlators early, prompt, and late I_E, I_P, I_L are used and feeding in the discriminator by calculating the difference between early and late correlators. Discriminator output then serves as feedback to adjust code delay and correlator outputs in a new round of iteration.

Discriminator output represents code tracking error. Under the assumption that auto-correlation is much larger than the cross-correlations, the normalized early-minus-late coherent discriminator can be written as [17]:

$$D = (I_E - I_L)/(I_E + I_L)/2$$
$$\cong \left(R_{cc}(-\frac{d}{2}) - R_{cc}(\frac{d}{2}) \right) / R_{ac}(-\frac{d}{2})/4 \qquad (7)$$

where d is correlator spacing in chips, $R_{cc}(\pm d/2)$ and $R_{cc}(\pm d/2)$ are cross-correlation and auto-correlation with early or late delays.

It is obvious that the tracking error is related to the correlator spacing. Like the white noise, using smaller d, cross-correlation components $R_{cc}(d/2)$ and $R_{cc}(-d/2)$ become dependent and the common part could be canceled out.

Furthermore, combining eq. (6) and (7), the property of dependency on Doppler offset will show up. Simulation is given on the cross-correlation effect on the code tracking accuracy when Doppler offset $\Delta f_{m,k}$ linearly increased over time from -2500 Hz to 2500 Hz. The integration time used in the simulation is 20 ms, and correlator spacing is 0.8 chips. Only one interference signal is assumed, and has the same power level with the desired signal.

As displayed in Figure 11, zero and n-kHz Doppler crossover phenomenon are easily observed from the output of discriminator. However, different crossing points give different error contributions. At the zero or 2-kHz crossing moments, the reaction of code error is a sudden change of up to 5 m, while 1-kHz crossing point introduces error at approximately 2 m. The error pattern is a sinusoidal-like oscillation around the crossover point. A sensitive zone of ±25 Hz around the crossover point can then be defined where cross-correlation contributes the largest errors.
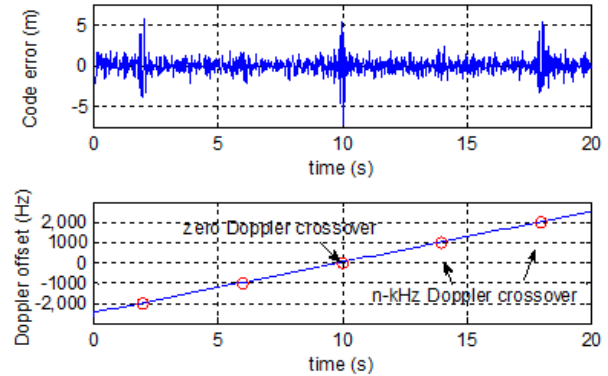

Figure 11. Code error estimation in presence of cross-correlation (top); Doppler offset between the desired and interfering signals, which is changing over time from -2500 Hz to 2500 Hz (bottom)

The cross-correlation error is not always as high as shown in Figure 11. According to eq. (6), it is also PRN code pattern and code delay dependent. RRN 7 and 22 are chosen with delay of 923 and 204 (1023 in total for C/A code) in this simulation after 1000 trials using Monte Carlo method. This code pattern and delay combination is at the moment when the average error plus standard variation is obtained.

It should be noted that the error magnitude is also affected by the code Doppler. Similar to the carrier Doppler offset, code Doppler offset also exists and will slowly change the relative delay between the desired and interfering signals, leading to the error magnitude being slightly enlarged or lessened. Randomly choosing code delays in Monte Carlo method can specifically illustrate the probability density distribution of the code Doppler effects in terms of code delay, which is however not shown in this paper in order to give a clear overview of the carrier Doppler crossover effect.

C. Near-far problem at Doppler crossover

The well-known near-far problem not only deteriorates the E_b/N_0 performance as displayed in Figure 11, but more seriously exacerbates the navigation accuracy, especially when it shows up at the moment of Doppler crossover.

Suppose the Doppler offset is 1 Hz, which is inside the sensitive zone of zero-Doppler crossover. Simulation in Figure 12 displays the errors when the interfering signal strength is linearly increased over time while the desired signal strength is constant. It is clear that cross-correlation error follows the sinusoidal-like oscillation at the frequency of 1 Hz, and the error magnitude also increases linearly.

That means the magnitude of cross-correlation error is proportional to the interfering/desired signal strength ratio. This relationship implies the same relevance between the

error and the inter-satellite distance diversity. Higher distance diversity in formation leads to poorer cross-correlations accordingly.
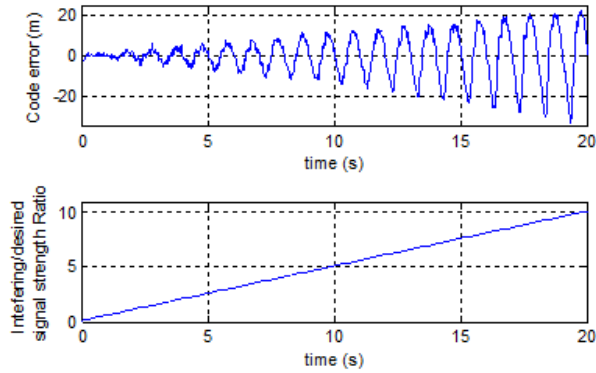

Figure 12. Code error estimation in presence of cross-correlation at 1 Hz Doppler offset (top); Inteference-to-desired signal strength ratio, which is changing over time from 0.1 to 10 (bottom)

VI. CASE STUDY: MAI EFFECTS IN FORMATION FLYING

Two case study scenarios are provided in order to evaluate the MAI effects in realistic formations.

A. Low earth orbit chief-deputy formation scenario

A formation geometry in the low earth orbit (LEO) with a chief satellite and several deputy satellites is a commonly used relative orbit geometry. In case of a Keplerian two-body motion, a circular chief orbit, and inter-satellite distance much smaller than the chief's semi-major axis, the relative dynamics can be expressed in Closhessy-Wiltshire (CW) equations in a linear form in Hill frame [25]. The relative motion of the deputy with respect to the chief is:

$$x = (r \ v)^T = (x \ y \ z \ \dot{x} \ \dot{y} \ \dot{z})^T \tag{8}$$

The vectors r and v denotes the relative positions and velocities in radial, along-track and cross-track directions. A safe ellipse relative orbit can be created and results in a closed form periodic solution when the initial orbit elements satisfy [25]

$$4x_0 + 2\dot{y}_0 / n = 0 \tag{9}$$

$$y_0 - 2\dot{x}_0 / n = 0 \tag{10}$$

where n is the orbital mean motion according to $n = (\mu/a^3)^{1/2}$, with μ the Earth's gravitational coefficient and a the semi-major axis of the chief. In such a safe ellipse orbit, the chance of collisions is minimized.

Suppose there are five satellites in formation, one is chief and the others are deputies in two safe elliptical orbits. The initial relative orbit elements are in Table I. The orbit of the chief is circular with a semi-major axis of 7000 km. After propagating the relative orbits using CW equations, it could be seen in Figure 13(a) that both of the relative orbits of deputy satellites are coplanar, which has an elliptical projections in the *xy*- and *xz*-plane, resulting in the linear

motion in the *yz*-plane. The ellipse for Sat 1 and Sat 2 has the dimensions of 1×1×1 km, while Sat 3 and Sat 4 are in a 1×2×2 km ellipse. Inter-satellite distance of each of the deputies with respect to the chief is also displayed in Figure 13(b) in the pattern of sinusoid.

TABLE I.   INITIAL RELATIVE ORIBT ELEMENTS

	x_0 [m]	y_0 [m]	z_0 [m]	$\dot{x}_0$ [m/s]	$\dot{y}_0$ [m/s]	$\dot{z}_0$ [m/s]
Sat 1	1000	0	0	0	-2.156	-0.178
Sat 2	587.78	-1618.03	-809.02	-0.872	-1.267	-0.634
Sat 3	-1000	0	0	0	2.156	2.156
Sat 4	-587.78	1618.03	1618.03	0.872	1.267	1.267
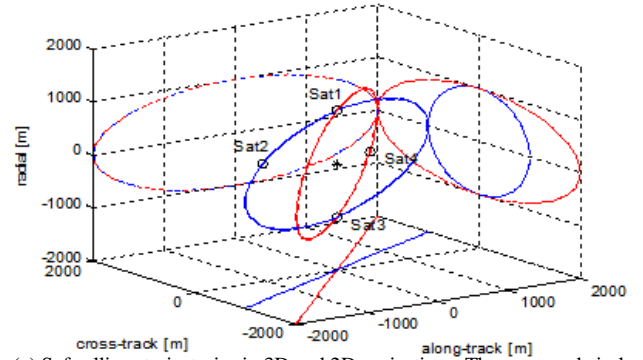
(a) Safe ellipse trajectories in 3D and 2D projections. The cross and circle denote the positions of the chief and deputies at t0, respectively.
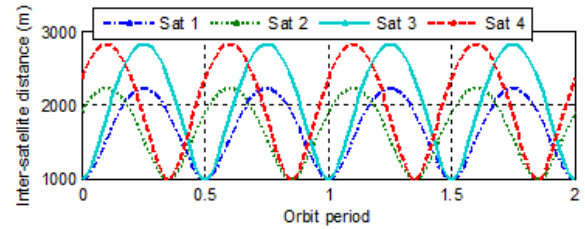
(b) Inter-satellite distance of each of the deputies with respect to the chief

Figure 13. Safe ellipse relative orbit propagation in five satellite formation

When the chief satellite receiving signals from the deputies at the same time in CDMA architecture, multiple access interference will occur that results from their cross-correlation effects. As analysed in last section, cross-correlation is signal strength and Doppler dependent. Signal strength ratio between the interfering and desired signal could be easily calculated by inversely scaling the inter-satellite distance ratio. Doppler frequency is:

$$\Delta f_D = \frac{f_{carrier}}{c} v'$$
$$= \frac{f_{carrier}}{c} \frac{v \cdot r}{|r|} = \frac{f_{carrier}}{c} \frac{\dot{x}x + \dot{y}y + \dot{z}z}{\sqrt{x^2 + y^2 + z^2}} \tag{11}$$

Note that v' is not the satellite orbiting velocity, but the velocity projected in the inter-satellite link direction. Only

this part of velocity will introduce Doppler to the inter-satellite link. Carrier frequency of the signal $f_{carrier}$ is assumed to be 2.4 GHz in S-band, and c is speed of light.

For the receiver on the chief, multiple channels are allocated to track different PRN codes from deputies. Suppose one of these channels is for Sat 3, then signals from Sat 1, 2, 4 are regarded as interfering signals. Figure 14 provides their signal strength ratio and Doppler offsets, as well as the code errors resulting from the contributions of cross-correlations accordingly.

The period of Doppler offset or signal strength ratio is half of the orbit period. We only look at the first half. Note that during the whole period, Doppler offset is within or quite close to the Doppler crossover sensitive zone of ±25 Hz. That leads to a large error being brought in to the inter-satellite ranging system.

Analysing the bottom plot in Figure 14 it is shown that in general cross-correlation errors oscillate with changing frequencies and changing magnitudes. Maximum errors occur at the measurement batch of [0.3, 0.4] orbits and a clear slow frequency fading moment around 0.32 orbits is visible. This is caused by the exact zero-Doppler crossings of $\Delta f_{D,23}$ and $\Delta f_{D,43}$ that are happened coincidently at the moment of their highest signal strength ratio. Another zero-Doppler crossings for $\Delta f_{D,23}$ and $\Delta f_{D,43}$ occur around 0.02 orbits, but at a much smaller magnitude, because the signal strength ratio at that time is around nadir.
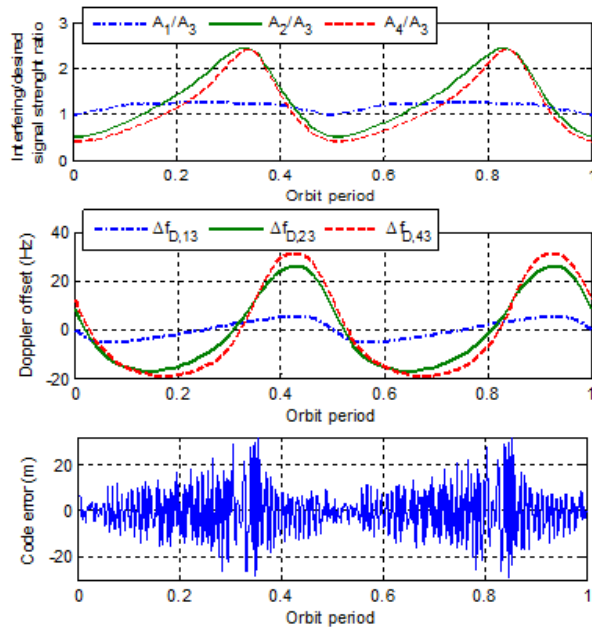

Figure 14. MAI effects in LEO safe ellipse formation geometry. Top: interfering/desired siganl magnitude ratio; Middle: Doppler offset; Bottom: code errors in presence of cross-correlations from 3 interfering Satellites.

B. Magnetospheric Multiscale formation scenario

MMS formation is a NASA mission, which uses four identical spacecraft to make three-dimensional measurements of magnetospheric boundary regions and examine the process of magnetic reconnection [4].
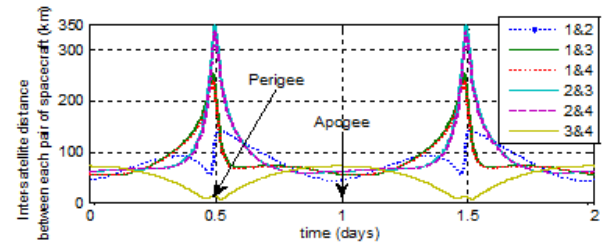
MMS mission has four identical spacecraft in a tetrahedral geometry. Inter-satellite communication will be conducted in a distributed topology and no signal spacecraft serves as chief. Two distinct phases will be in this mission. For Phase 1, MMS will be in a 1.2×12 Earth Radii highly elliptical orbit with a period of approximately one day. The initial orbital elements can be found in [4].

Unlike the low earth circular orbit in the last scenario, MMS mission cannot use linearized CW equations for relative orbit determination, but by propagating the absolute orbits of all the spacecraft using absolute Keplerian dynamics and then determining the relative motion in the Hill frame using a standard transformation.

Figure 15(a) displays the relative trajectories of Sat 2, 3, 4 with respect to Sat 1 to give a basic overview on how do they perform tetrahedral formation. Figure 15(b) exhibits their inter-satellite separation between each pair of spacecraft over two complete orbits. Near apogee, the inter-satellite distance are generally about 60 km, but near perigee, the spacecraft separations vary dramatically, which can be as large as 350 km and as small as 10 km.
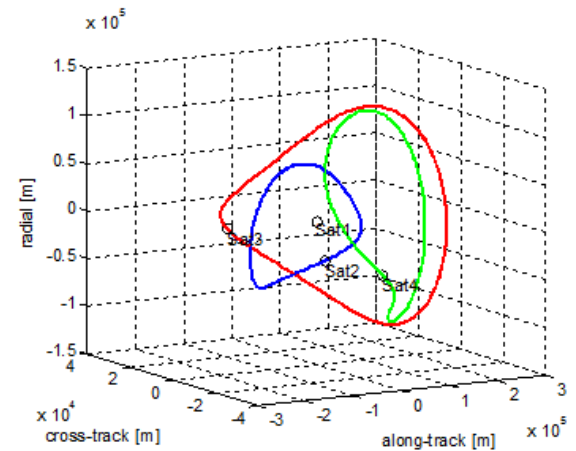
(a) MMS mission relative trajectories in 3D of Sat 2, 3, 4 with respect to Sat 1. The circle denotes the positions of the four identical spacecraft at t_0.

(b) Inter-satellite distance between each pair of the spacecraft in MMS.

Figure 15. MMS mission relative orbit

MMS mission, with four purely identical and distributed spacecraft, is a good example of implementing CDMA with roles rotating architecture. At a flexible time slot, one of the spacecraft will be regarded as reference and receiving signals from the other three simultaneously. That indicates the potentials of multiple access interference. Furthermore, high distance diversity at perigee is particularly challenging for

CDMA architecture in the sense of near-far problem. It is valuable to investigate the most critical moments when the cross-correlation contributes the largest errors within a whole orbit period for MMS mission.

Figure 16 gives two examples of Sat 1 and Sat 4 as receivers, respectively, at two distinct time slots when interfering/desired signal arrived at receivers with dramatically different signal strength ratio.

The first example in Figure 16(a) shows maximum 4 times signal strength ratio, as well as the corresponding Doppler offset from minimum of -220 Hz to maximum of 800 Hz (blue dash line). Doppler offset is far beyond the Doppler crossover sensitive zone most of the time except for the crossing moments at around 0.20 and 0.92 days, when the slow frequency fading cross-correlation errors can be observed in the bottom figure. Interference at the duration of [0.38, 0.50] days, even with high signal strength ratio, should not contribute much more errors since the Doppler offset is extremely far from crossover. The visible errors at that duration actually come from the other interference contributor (green solid line) with its crossover at around 0.5 days and its general Doppler distribution all within the sensitive zone.
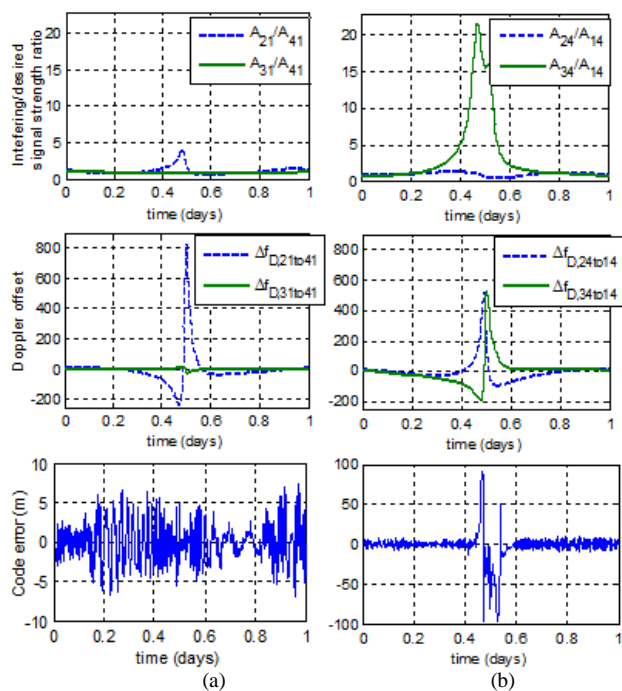

Figure 16. MAI effects in MMS mission. Top: interfering/desired siganl magnitude ratio; Middle: Doppler offset; Bottom: code errors in presense of cross-correlations when (a) Sat 1 is as receiver, requiring ranging signal from Sat 4 but interfered by Sat 2 and 3; (b) Sat 4 is as receiver, obtaining ranging signal from Sat 1 but interfered by Sat 2 and 3.

The other example in Figure 16(b) occurs more often because of the widely diverse inter-satellite separations, leading to severe near-far problem with up to 23 times signal strength ratio. This results in the degradation of the signal per bit to noise density reaching its bad performance threshold as explained before, but also yielding significant cross-correlation errors even if the corresponding Doppler offset beyond crossover sensitive zone. Up to 100 m errors are visible for a measurement batch of [0.45, 0.55] days. During that time, a Doppler crossover at around 0.50 days does happen, but luckily, is very instantaneous and almost does not leave even more severe consequences. The error magnitude is not proportionally increasing with the change of signal strength ratio, but keeping low due to the compensation by the large Doppler offset. The first error spike shows up when the signal strength ratio reaches 13. That indicates a kind of threshold for the occurrence of significant errors regardless of Doppler offset.

C. Case-study summary

The effects of near-far problem and Doppler crossover play important roles in defining the CDMA capability for the combined inter-satellite communication and navigation.

In case of low diverse inter-satellite separations, e.g., the scenario of safe ellipse orbit in LEO, the corresponding Doppler offset is diminutive, leading to high occurrence of zero-Doppler crossover and considerable MAI errors within the whole orbit period.

In case of high diverse inter-satellite separations, e.g., the scenario of MMS mission in highly elliptical orbit, Doppler offset is much higher and beyond the crossover sensitive zone for a substantial time of an orbit period, resulting in smaller cross-correlation errors. However, if the distance ratio between spacecraft reaches to the extent that even the large Doppler offset cannot compensate its influence any longer, significant errors will show up and affect the system accuracy to a large degree. To this end, an adaptive power control mechanism could be useful to minimize the impact of near-far problem, which ideally implements dynamically adjustable power attenuation in order to lower the transmitting power of interfering signals when they are in the close proximity.

Note that for both scenarios, there is no n-kHz Doppler crossover taking place. However, if thinking of going to higher carrier frequency, e.g., K-band or Ku-band, for the same orbit relative geometry, the chance of n-kHz Doppler crossover is getting high, which is also a resource of large MAI errors.

The methods of mitigating the MAI errors include an improvement of code delay loop inside the receiver by using a smaller correlator spacing or a longer integration time. One can also think of long time carrier phase smoothing of the pseudorange measurements, but should carefully take into account the requirements of high code and phase update rate in such PFF missions.

VII. CONCLUSIONS

In this paper, several network architectures are presented to support inter-satellite communication and relative navigation for PFF missions. Different multiple access technologies, half-duplex/full duplex configurations and network topologies are thoroughly analysed and combined as potential networking solutions for PFF missions. The

dedicated requirements for PFF missions are proposed, including the time critical issue and the operational flexibility, which are used as criteria to evaluate different architectures. Half-duplex CDMA with roles rotating is selected as a suitable architecture, as it enables system working with a wide range of flexibility, such as enabling both code and carrier phase measurements at variable mission phases, allowing to detect some spacecraft while tracking others, and being insensitive to a spacecraft joining in or dropping out of the formation. GNSS-like technology can also be utilized to the largest extent in CDMA network.

The limitation of using CDMA is investigated in terms of the Multiple access interference. This interference is Doppler dependent and suffers as well from the near-far problem. Regarding the communication performance, it is shown that the equivalent energy per bit to noise density ratio is reduced as compared to the case without MAI, leading to a limited inter-satellite separation diversity and a limited maximum number of spacecraft in the formation. Furthermore, MAI error worsens the navigation accuracy, especially at the moment of zero- or n-kHz Doppler crossovers or in case of signals being corrupted by the near-by interferences. Two case-study scenarios, one of a low earth circular orbit mission and another for a highly elliptical orbit mission, are provided that verifies the severe effects of MAI and the high probability of its occurrence within an entire orbit period.

MAI errors easily exceed the meter level, which can be mitigated using smaller correlator spacing or longer integration time. Long time carrier smoothing is also helpful to minimize the MAI errors. However, the requirements on the high update rates of the code and carrier phases need to be carefully taken into account in some tight control periods in the PFF missions.

REFERENCES

[1] R. Sun, J. Guo, E. Gill and D. Maessen, "Characterizing network architecture for inter-satellite communication and relative navigation in precise formation flying", 3rd International Conference on Advances in Satellite and Space Communications (SPACOMM 2011), Budapest, Hungary, 17-22 April, 2011.

[2] A. Wishart, F. Teston, et al. "The PROBA-3 Formation Flying technology Demonstration Mission", 58th International Astronautical Congress, Hyderabad, India, 24-28 September 2007.

[3] C. Bourga, C. Mehlen, et al. "A Formation Flying RF Subsystem for DARWIN and SMART-2", International Symposium Formation Flying: Missions & Technologies, Toulouse, France, 29-31 October 2002.

[4] M. Volle, T. Lee and A. Long, "Maneuver Recovery Analysis for the Magnetospheric Multiscale Mission", NASA Technical Reports Server, 2007.

[5] J. Y. Tien, J. M. Srinivasan, L. E. Young, et al, "Formation acquisition sensor for the Terrestrial Planet Finder (TPF) mission", IEEE Aerospace Conference, Big Sky, Montana, 6-13 March, 2004.

[6] V. Barrena, M. Suatoni, C. Flores, J. Thevenet and C. Mehlen, "Formation flying RF ranging subsystem for RPISMA: navigation algorithm design and implementation", Proc. 3rd Int. Symposium on Formation Flying, Missions and Technologies, Noordwijk, the Netherlands, 23-25 April 2008.

[7] G. Heckler, L. Winternitz, W. Bamford, "MMS-IRAS TRL-6 Testing", ION GNSS 2008, Savannah, GA, 16-19 Sep. 2008.

[8] J. Bristow, "A Formation Flying Technology Vision", AIAA Space Conference and Exposition, Long Beach, CA, 19-21 Sep. 2000.

[9] K. Hogie, E. Criscuolo and R. Parise, "Using standard Internet Protocols and Applications in Space", Journal of Computer Networks, vol. 47, 2005, pp. 603-650.

[10] L. Wood, W. Ivancic, D. Hodgson, et al, "Using Internet Nodes and Routers onboard Satellites", International Journal of Satellite Communications and Networking, vol. 25, no. 2, 2007, 195-216.

[11] R. Slywczak, "Low-Earth-Orbit Satellite Internet Protocol Communications Concept and Design", NASA/TM technical report, 2004-212299.

[12] T. Vladimirova, C. P. Bridges, G. Prassions, et al, "Characterising Wireless Sensor Motes for Space Applications", 2nd NASA/ESA Conference on Adaptive Hardware and Systems (AHS 2007), Edinburgh, UK, 5-8 Aug. 2007, pp. 43-50

[13] T. Vladimirova, X. Wu, C. P. Bridges, "Development of a Satellite Sensor Network for Future Space Missions", IEEE Aerospace Conference, Big Sky, MT, 1-8 March, 2008, pp. 1-10

[14] P. Dubois, C. Botteron, V. Mitev, et al, "Ad-hoc Wireless Sensor Networks for Exploration of Solar-System Bodies", Acta Astronautica, vol. 64, 2009, pp. 626-643

[15] P. Brenner, "A Technical Tutorial on the IEEE 802.11 Protocol", Breezecom Wireless Communications, 1997.

[16] A. J. Van Dierendonck, G. A. McGraw, R. J. Erlandson and R. Coker, "Cross-correlation of C/A codes in GPS/WAAS Receivers", ION GPS 99, Nashville, TN, 14-17 Sep. 1999.

[17] Z. Zhu and F. Van Graas, "Effects of Cross Correlation on High Performance C/A Code Tracking", ION NTM 2005, San Diego, CA, 24-26 Jan. 2005.

[18] E. Gill, O. Montenbruck, K. Arichandran, S. Tan and T. Bretschneider, "High-precision onboard orbit determination for small satellites-the GPS-based XNS on X-SAT", 6th Symposium on Small Satellites Systems and Services, La Rochelle, France, 20-24 Sep. 2004.

[19] L. P. Clare, J. L. Gao, E. H. Jennings and C. Okino, "A Network Architecture for Precision Formation Flying Using the IEEE 802.11 MAC Protocol", IEEE Aerospace Conference, Big Sky, MT, 5-12 March 2005.

[20] R. Sun, D. Maessen, J. Guo and E. Gill, "Enabling inter-satellite communication and ranging for small satellites", 9th Symposium on Small Satellites Systems and Services, Funchal, Portugal, 31 May – 4 June, 2010.

[21] J. Kim and B. Tapley, "Simulation of dual one-way ranging measurements", Journal of spacecraft and rockets, vol. 40, 2003, pp. 419-425.

[22] J. Spilker, "Signal structure and theoretical performance", Global Positioning System: Theory and Applications, American Institute of Aeronautics and Astronautics, Inc. vol. 1, 1996, pp. 57-105.

[23] P. Ward, J. Betz and C. Hegarty, "GPS satellite signal characteristics", Understanding GPS: Principles and Applications, 2nd ed., Artech House, Inc. 2006, pp. 135-145.

[24] M. Pratap and P. Enge, Global Positioning System: Signals, Measurements and Performance, 2nd ed., Ganga-Jamuna Press, 2006, pp. 365-379.

[25] K. Alfriend, S. R. Vadali, P. Gurfil, J. How and L. Breger, "Spacecraft Formation Flying – Dynamics, Control and Navigation", 1st ed., Elsevier, 2010, pp. 84-89.